International Journal of Design & Nature and Ecodynamics
Vol. 21, No. 10, October, 2026, pp. 2909-2919
Journal homepage: http://iieta.org/journals/ijdne

Preliminary Assessment of Patchouli Essential Oil Concentration on the Structure and Performance of Durian-Seed-Starch Biofilms

Irhamni[1*], Saudah[2], Andika Munandar[1], Yuni Lisafitri[1], Fadlan Hidayat[3]

[1] Department of Environmental Engineering, Faculty of Infrastructure and Regional Technology, Institut Teknologi Sumatera, Lampung 35376, Indonesia
[2] Department of Biology Education, Postgraduate Program, Universitas Serambi Mekkah, Banda Aceh 23123, Indonesia
[3] Department of Agricultural Industrial Engineering, Faculty of Agricultural Technology, Universitas Serambi Mekkah, Banda Aceh 23123, Indonesia

Corresponding Author Email: irhamni@tl.itera.ac.id

Copyright: ©2026 The authors. This article is published by IIETA and is licensed under the CC BY 4.0 license (http://creativecommons.org/licenses/by/4.0/).

https://doi.org/10.18280/ijdne.211006

Received: 3 August 2026
Revised: 14 October 2026
Accepted: 23 October 2026
Available online: 31 October 2026

Keywords:
durian seed starch, patchouli essential oil, biodegradable film, tensile properties, thermal degradation

ABSTRACT

Durian seed starch is a renewable matrix for biodegradable films, while patchouli essential oil (PEO) may modify their properties. This study examined the effects of PEO concentration on durian seed starch films. Starch was extracted from durian seed residues, and films were cast at PEO loadings of 0.37, 0.75, 1.10, and 1.50 mL/100 mL of film-forming solution (S1–S4, respectively). Films were characterized using Fourier-transform infrared (FTIR), scanning electron microscopy (SEM), thickness measurement, tensile testing, and thermogravimetric analysis coupled with derivative thermogravimetry (TGA–DTG). FTIR spectra retained the characteristic starch bands, with no distinct new bands detected. SEM showed localized surface heterogeneities without a clear progressive increase in surface disruption. Film thickness decreased from 0.53 to 0.24 mm, while the individual tensile-strength values increased from 0.647 to 1.215 MPa; thickness was similar for S3 and S4. The single-run TGA–DTG profiles showed non-monotonic differences: S3 had the highest $T_{5\%}$ and $T_{10\%}$, the lowest maximum mass-loss rate, and the highest residue at 600 °C, whereas S4 had the highest T_{max} (326.15 °C). Overall, the measured properties differed among the four PEO-containing formulations, with S3 showing the most balanced profile within the tested loading range. Because no oil-free control was included, these findings do not establish the net effect of PEO addition.

1. INTRODUCTION

Conventional food packaging still relies heavily on petroleum-derived plastics because of their favorable mechanical strength, ease of processing, and barrier performance [1, 2]. However, the persistence of these materials after disposal, together with concerns related to plastic accumulation, microplastic formation, greenhouse gas emissions, and resource depletion, has intensified efforts to develop packaging materials from renewable and biodegradable sources [3-5]. Biopolymer-based materials have therefore gained increasing attention as potential alternatives to conventional plastics, particularly because many can be obtained from renewable biomass and exhibit inherent biodegradability and biocompatibility [6-8]. Among these materials, starch is considered one of the most promising film-forming biopolymers because it is abundant, renewable, relatively inexpensive, and available from a wide range of botanical and agricultural sources [4, 6, 9]. Its molecular structure also enables the formation of continuous film matrices, making starch a versatile platform for the development of biodegradable film materials [5]. Nevertheless, the properties of starch-based films remain strongly dependent on starch source, formulation, and incorporated additives, providing considerable scope for tailoring their performance for specific applications [6, 9].

Durian processing generates substantial amounts of seed residues that are often underutilized despite their potential as value-added biomaterials. Durian seeds are rich in starch and mucilage, making them a promising renewable feedstock for the development of film-forming materials [10, 11]. The valorization of durian seed starch into biodegradable films therefore offers an opportunity to convert agricultural residues into more sustainable polymeric materials, and durian seed starch has already been explored for edible-film applications [11]. However, starch-based films generally exhibit limitations in structural stability and mechanical performance, while their properties are strongly influenced by starch source, processing conditions, plasticization, and other incorporated additives [9].

Glycerol is commonly incorporated into starch-based films as a plasticizer because its low molecular weight and hydroxyl groups facilitate interactions with starch chains, reducing brittleness and improving film flexibility and processability

[12]. However, plasticization alone does not fully overcome the inherent limitations of starch films, particularly in terms of mechanical and thermal performance. Consequently, additional modification strategies, including the incorporation of essential oils and other functional additives, have been increasingly explored to tailor the structure and overall properties of starch-based films [9]. Patchouli essential oil (PEO), obtained from *Pogostemon cablin*, is a complex essential oil rich in sesquiterpenes, with patchoulol identified as its major constituent [13]. When incorporated into polymeric matrices, its hydrophobic oil phase and constituent compounds may modify intermolecular interactions and polymer-chain organization.

Studies on starch-based films have examined patchouli-derived additives in different film matrices and formulations. Patchouli oil was incorporated into poly(vinyl alcohol) (PVA)/corn starch hydrogel films containing silver nanoparticles biosynthesized using patchouli leaf extract [14]. In breadfruit starch biofilms, varying the concentration of PEO was used to assess its effects on physical and mechanical properties and antibacterial activity [15]. In durian seed starch films, starch concentration was varied while the amount of patchouli leaf extract was held constant [16]. Response surface methodology was also used to formulate durian seed starch biocomposite films containing nanocrystalline cellulose and carrageenan [17]. Together, these studies provide a basis for using patchouli-derived additives and modifying durian seed starch film matrices, with each study addressing a different formulation question.

Accordingly, the contribution of the present study lies in the comparative evaluation of how different nominal PEO loadings are associated with structural, morphological, mechanical, and thermal differences in durian seed starch films. Unlike the fixed patchouli leaf-extract formulation in a previous study [16] and the nanocellulose/carrageenan reinforcement strategy in a previous study [17], the present study examines four PEO-containing formulations and evaluates their Fourier-transform infrared (FTIR) characteristics, surface morphology, film thickness, tensile strength (TS), and thermal degradation behavior. In relation to a previous study [15], which investigated concentration-dependent PEO responses in breadfruit-starch films, the present work extends this comparative assessment to durian seed starch and considers molecular, morphological, mechanical, and thermal characteristics together. This approach provides an opportunity to examine whether the measured properties exhibit consistent or distinct patterns across the investigated PEO loadings. Therefore, this study aimed to compare the structure–property relationships of durian seed starch films prepared with four PEO loadings (0.37, 0.75, 1.10, and 1.50 mL/100 mL of film-forming solution). The investigation focused on film thickness, TS, FTIR spectral features, surface morphology, and thermal degradation behavior. We hypothesized that differences in PEO loading would be associated with distinct, potentially non-linear changes in the structural, mechanical, and thermal properties of the resulting films.

2. MATERIALS AND METHODS

2.1 Materials

Approximately 5 kg of durian seeds were collected during a single collection campaign from several vendors in Banda Aceh, Indonesia. The seeds originated from post-consumption residues and multiple sales batches and were pooled into one composite batch for starch extraction. The botanical varieties of the collected seeds could not be reliably identified because the seeds were obtained from mixed discarded residues. The composite batch was used as a common raw-material source for all subsequent film formulations to maintain consistency of the starch source within the experimental series. PEO was obtained from the Atsiri Research Center (ARC), Universitas Syiah Kuala, Banda Aceh, Indonesia. A batch-specific certificate of analysis or compositional certificate was not available for the oil used in this study. Therefore, its batch-specific chemical composition was not independently verified, and the discussion of its effects was not attributed to individual chemical constituents. Analytical-grade glycerol was used as the plasticizer, sodium chloride (NaCl) was used during starch extraction, and distilled water was used throughout the extraction and film-preparation processes.

2.2 Extraction and physicochemical characterization of durian seed starch

The collected durian seeds were thoroughly washed with water to remove adhering residues and then manually peeled to remove the seed coat. The peeled seeds were cut into small pieces and homogenized using a blender (Miyako, Indonesia). During homogenization, NaCl was added at a ratio of 3 g per 100 g of seed material to minimize browning during processing.

The resulting slurry was placed on a filter cloth positioned over a collection vessel and manually pressed and rinsed with water. This procedure allowed the starch-containing liquid fraction to pass through the cloth while retaining coarse fibrous material. The collected filtrate was left undisturbed for 24 h to allow complete sedimentation of the starch. The supernatant was subsequently removed, and the recovered starch sediment was dried in an oven at 40 °C for 24 h. The dried starch was then used for physicochemical characterization and subsequent film preparation.

Table 1. Physicochemical characteristics of the extracted durian seed starch

Parameter	Unit	Result	Method
Moisture content	%	7.79	Gravimetric
Ash content	%	1.66	
Fat content	%	0.17	Soxhlet
Protein content	%	5.56	Kjeldahl
Carbohydrate	%	84.82	By difference
Crude fiber	%	2.85	Gravimetric
Color, L*	–	92.26	CR-300 Chromameter
Color, a*	–	6.02	
Color, b*	–	3.90	
Amylose content	%	21.56	SNI 6128:2015

Note: SNI stands for Standar Nasional Indonesia (Indonesian National Standard). SNI 6128:2015 specifies rice quality requirements and testing procedures, including spectrophotometric determination of amylose content (Section 7.11).

The isolated durian seed starch used for film preparation was submitted to the BRMP Pascapanen Pertanian Laboratory, under the Ministry of Agriculture of the Republic of Indonesia, for physicochemical characterization (Laboratory report No. 3/LBBPSC/VI/26). According to the report, moisture and ash contents were determined gravimetrically, crude fat using the

Soxhlet method, crude protein using the Kjeldahl method, and crude fiber gravimetrically. Total carbohydrate was calculated by difference rather than measured directly (Eq. (1)). Color parameters (L*, a*, and b*) were determined using a CR-300 chromameter, while amylose content was reported using the method specified as SNI 6128:2015. The physicochemical characteristics were analyzed in a single run without replication. The resulting physicochemical characteristics were used to describe the isolated starch material employed in film preparation. The physicochemical characteristics of the extracted durian seed starch used as the film-forming material are summarized in Table 1.

$$\text{Carbohydrate (\%)} = 100 - (\text{moisture} + \text{ash} + \text{fat} + \text{protein}) \quad (1)$$

2.3 Preparation of durian seed starch films containing patchouli oil

Durian seed starch films were prepared by solution casting using previously reported methods [17, 18], with modifications to the formulation and processing conditions. For each formulation, the entire 100 mL film-forming dispersion was cast onto a single 20 × 20 cm glass plate, producing one film sheet per formulation. All four cast films were dried simultaneously in the same hot-air oven at 60 °C for 24 h. After drying, the films were carefully peeled from the glass plates and conditioned in a desiccator prior to characterization. The effective area covered by each film and the final dry mass were not recorded. Representative stages of the film-preparation process are shown in Figure 1. The compositions of the four formulations are summarized in Table 2.

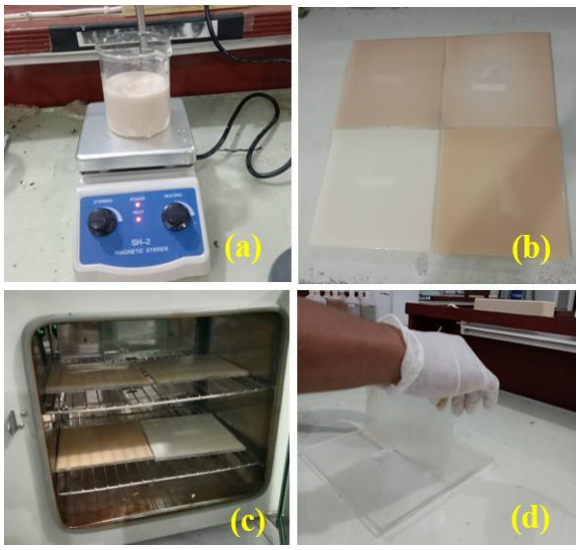

Figure 1. Representative photographs of the preparation of durian seed starch films containing patchouli essential oil (PEO): (a) preparation and homogenization of the film-forming dispersion, (b) resulting film samples, (c) oven drying of the cast films, and (d) removal of the dried film from the casting plate

All four formulations contained PEO, and an oil-free starch-glycerol control was not included in the experimental design. Accordingly, the present study was designed to compare differences among the four PEO-containing formulations rather than to determine the net effect of PEO addition relative to a PEO-free starch-glycerol matrix.

Durian seed starch was first dispersed in distilled water and heated to 90 °C under continuous stirring at 100 rpm for 20 min to promote starch gelatinization and produce a uniform film-forming matrix. Glycerol and PEO were subsequently incorporated according to the formulation design, followed by an additional 10 min of stirring at 100 rpm to facilitate their incorporation into the starch-based dispersion. The resulting dispersion was cast onto a 20 × 20 cm glass plate and spread evenly over the casting surface. The films were dried in a hot-air oven at 60 °C for 24 h. After drying, the films were carefully removed from the glass plates and conditioned in a desiccator before characterization.

The PEO loadings reported in this study represent the nominal volumes initially introduced into the film-forming formulations. The amount of PEO retained in the dried films was not quantified; therefore, the reported values should not be interpreted as the actual residual oil content after film processing.

Table 2. Composition of durian seed starch film-forming formulations

Sample	Durian Seed Starch (g/100 mL)	Nominal PEO Loading (mL/100 mL)	Glycerol (mL/100 mL)
S1	9.75	0.37	3.00
S2	9.75	0.75	3.00
S3	9.75	1.10	3.00
S4	9.75	1.50	3.00

Note: Patchouli essential oil (PEO) loadings represent the nominal volumes added to the initial film-forming formulations, rather than the measured oil contents retained in the dried films. All formulations were prepared to a final volume of 100 mL.

2.4 Characterization of the films

2.4.1 Film thickness

Film thickness was measured using a digital micrometer at three spatially separated positions within each of three sections obtained by dividing the dried film sheet. For each section, the mean of the three individual measurements was calculated to obtain one section-level thickness value (U1–U3). The overall thickness for each formulation was subsequently expressed as the mean ± standard deviation of the three section-level values. Thus, the three values represent spatial subsamples from a single film sheet rather than independent film-production replicates. Accordingly, the reported standard deviation reflects within-film spatial variability only.

2.4.2 Fourier-transform infrared spectroscopy

FTIR spectroscopy was used to investigate changes in the functional groups and intermolecular interactions of the films associated with differences in patchouli oil concentration. The spectra were recorded using an FTIR-650 spectrometer (Tianjin Gangdong Technology Development Co., Ltd., China). FTIR spectra were recorded in attenuated total reflectance (ATR) mode over the range of 400–4000 cm^{-1}. The exported spectra were expressed as transmittance (%T) and plotted using OriginPro 2024 without additional spectral normalization.

2.4.3 Scanning electron microscopy

The surface morphology of the films was examined using scanning electron microscopy (SEM; JSM-6390LA, JEOL, Japan) at an accelerating voltage of 12 kV. Before imaging,

the specimens were mounted on aluminum stubs and sputter-coated with a nominal gold layer thickness of 10 nm to improve surface conductivity. Secondary-electron images were acquired at magnifications of 300× and 1000×, corresponding to scale bars of 50 and 10 µm, respectively. One specimen from each formulation was examined in a single SEM session, with one field of view recorded at each magnification. The available micrographs were therefore used for qualitative morphological comparison rather than statistical evaluation of surface features. Replicate SEM examinations across independent casting batches were not performed.

2.4.4 Thermogravimetric analysis

Thermogravimetric analysis (TGA) was performed using a DTG-60 thermal analyzer (serial no. C30564800501TK). For each formulation, a sample mass of 15.000 mg was placed in an aluminum cell and heated to 600 °C at a heating rate of 40 °C min^{-1} under a nitrogen atmosphere with a flow rate of 20 mL min^{-1}. No isothermal holding period was applied at the final temperature. The mass-loss profiles were recorded as a percentage of the initial sample mass. Derivative thermogravimetry (DTG) curves were obtained by calculating the first derivative of the corresponding TGA data and were used to identify the maximum mass-loss rate and the associated degradation temperature. The characteristic parameters evaluated included the temperatures corresponding to 5% and 10% mass loss ($T_{5\%}$ and $T_{10\%}$), the temperature of maximum degradation rate (T_{max}), maximum DTG rate, mass remaining at T_{max}, and residual mass at 600 °C. Each formulation was analyzed once (n = 1); therefore, the reported values represent individual measurements rather than replicate means, and no estimates of experimental variability or inferential statistical comparisons were calculated. The available instrument record did not specify whether a separate baseline correction was applied.

2.4.5 Tensile properties

The mechanical properties of the films were evaluated according to DIN EN ISO 527-1 using a Universal Testing Machine ZWICK ROELL 250 kN All Round. One specimen was tested for each formulation. The reported specimen widths were 27, 28, 29, and 27 mm for S1, S2, S3, and S4, respectively, while the corresponding specimen thicknesses were 0.53, 0.37, 0.25, and 0.24 mm. TS was calculated from the maximum recorded force divided by the initial cross-sectional area, according to Eq. (2):

$$TS(MPa) = \frac{F_{max}}{A_0} \quad (2)$$

where, TS is the tensile strength (MPa), F_{max} is the maximum tensile force recorded during testing (N), and A_0 is the initial cross-sectional area of the specimen (mm^2), calculated as the product of specimen width and thickness.

2.5 Statistical analysis

Film thickness was summarized descriptively as the mean ± standard deviation of three section-level measurements per formulation, with each section-level value representing the average of three spatial measurements. As only one film sheet was produced per formulation, these measurements represent within-film spatial subsamples rather than independent experimental replicates. TS was reported as an individual measurement for each formulation because only one specimen was tested per formulation. Accordingly, no inferential statistical tests were performed to compare film thickness or TS among formulations. The results were interpreted descriptively, taking into account the limited experimental replication.

3. RESULTS AND DISCUSSION

3.1 Fourier-transform infrared spectral characteristics and possible intermolecular interactions

The ATR-FTIR spectra of the durian seed starch films containing different concentrations of PEO are presented in Figure 2. All formulations exhibited broadly similar spectral profiles, with characteristic absorption features identified at approximately 3395–3406, 2932–2936, 1636–1647, 1389–1406, and 1013–1018 cm^{-1}. The exported spectra were plotted as transmittance (%T) without additional normalization in OriginPro 2024. The preservation of these characteristic absorption regions indicates that the principal functional-group features of the starch-based matrix remained detectable across all four formulations. However, because no oil-free starch–glycerol reference was included, the present comparison is restricted to differences among PEO-containing formulations and cannot isolate the spectral effect of PEO addition relative to the oil-free matrix. Lemos et al. [19] reported comparable preservation of characteristic starch-associated bands in potato starch films containing citrus essential oils, where the spectra retained broadly overlapping profiles without the appearance of distinct additional bands.

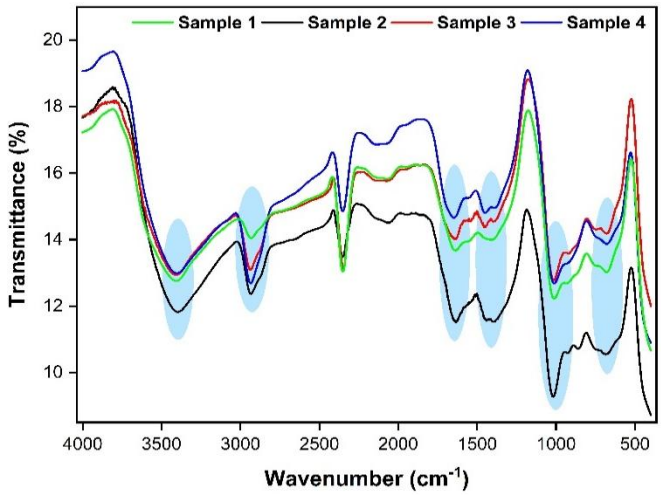

Figure 2. Attenuated total reflectance (ATR)–Fourier-transform infrared (FTIR) spectra (transmittance, %T) of durian seed starch films containing different concentrations of patchouli essential oil (PEO): S1 (0.37 mL/100 mL), S2 (0.75 mL/100 mL), S3 (1.10 mL/100 mL), and S4 (1.50 mL/100 mL)

The broad absorption band near 3400 cm^{-1} is attributed primarily to O–H stretching of hydroxyl groups in starch and glycerol and to residual water in the film matrix. A similar O–H stretching band at 3100–3700 cm^{-1} was reported for plasticized starch systems [20], and a comparable region was observed in starch/alginate films containing lemongrass

essential oil [21]. In the present study, the O–H peak positions ranged from 3394.72 to 3406.29 cm^{-1} and showed no consistent trend with PEO concentration. Residual moisture and variations in sample–crystal contact during ATR measurements may affect the band profile. Comparisons of absolute band intensities in the unnormalized transmittance spectra are therefore insufficient to establish systematic changes in hydrogen-bond strength. The persistence of the band is consistent with the presence of hydroxyl-rich constituents in the film matrix. Hydrogen-bonding interactions reported in PVA/corn starch films containing patchouli oil provide context for possible intermolecular associations in the present films [14].

The band at 2932–2936 cm^{-1} is assigned to aliphatic C–H stretching, with contributions from CH_2 and CH_3 groups in starch, glycerol, and PEO. Comparable bands were reported at 2933 cm^{-1} in starch/alginate films containing lemongrass essential oil [21] and at 2926 cm^{-1} in starch films containing citrus essential oils [19]. The feature at 1636–1647 cm^{-1} is attributed primarily to bending vibrations of bound or adsorbed water in the starch matrix, consistent with the assignment for plasticized starch films [20]. Residual protein may also contribute overlapping amide vibrations, given the protein content of 5.56% in the extracted durian seed starch (Table 1). The band at 1389–1406 cm^{-1} is associated with O–H and aliphatic C–H bending, while the prominent band at 1013–1018 cm^{-1} is assigned mainly to C–O and C–O–C stretching in the anhydroglucose units and glycosidic linkages of starch. Related starch absorptions have been reported at 1020–1089 cm^{-1} in plasticized starch films [20] and at 1150, 1084, and 1027 cm^{-1} in starch/alginate films [21].

The spectral response observed in the present study differs from that reported by Marta et al. [15] for breadfruit starch films containing PEO, in which concentration-dependent redshifts and an additional absorption band near 1735 cm^{-1} were reported at higher oil concentrations. In the present durian seed starch films, no comparably distinct additional band was identified in this region. Such differences may be associated with variations in starch botanical origin, formulation composition, oil loading, and film-processing conditions. Previous investigations of starch-based films containing essential oils have also reported that spectral changes may occur mainly through variations in existing absorption profiles rather than the appearance of distinct new functional-group bands [19, 21]. Nevertheless, the absence of an additional characteristic band should not be interpreted as definitive proof of a particular incorporation mechanism or as evidence that all possible chemical changes are absent.

Overall, the FTIR results demonstrate that the principal starch-associated spectral features remained recognizable across the four PEO-containing formulations, with modest variations in the positions and profiles of existing absorption bands. These variations did not exhibit a consistent concentration-dependent pattern and therefore do not establish systematic changes in hydrogen-bonding strength or molecular rearrangement. The available spectra also provide no distinct evidence of newly formed covalent functionalities. Accordingly, FTIR supports the preservation of the characteristic chemical features of the starch-based matrix, while the specific nature and extent of intermolecular interactions involving PEO remain unresolved. The use of the same extracted starch batch across all formulations also means that its residual non-starch constituents represented a common matrix background; however, their individual contributions to overlapping absorption bands cannot be separated using the available spectra.

3.2 Surface morphology and microstructural organization

The surface morphology of the durian seed starch films was examined at 300× and 1000× magnification to provide qualitative comparisons of the surface features among formulations containing different nominal PEO loadings (Figure 3). At 300×, the selected fields of all four formulations showed generally continuous surface backgrounds, accompanied by isolated particulate and irregular features. At 1000×, localized morphological differences were more apparent. S1 exhibited irregular surface domains and scattered particulate features, whereas S2 showed several localized depression-like and cavity-like regions. S3 contained a conspicuous elongated surface feature together with smaller discrete domains, while S4 exhibited scattered particulate and irregular surface features against a comparatively continuous background. These observations indicate that the selected surface fields differed in their local morphology; however, they do not establish a systematic concentration-dependent progression in surface roughness, porosity, or matrix continuity.

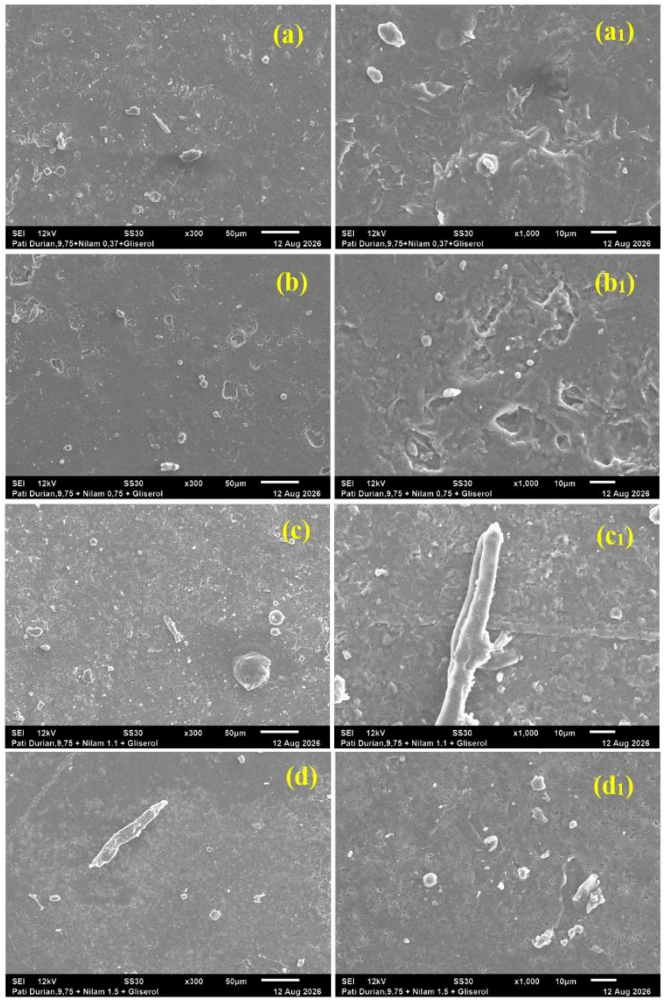

Figure 3. Selected scanning electron microscopy (SEM) images of durian seed starch films containing different nominal concentrations of patchouli essential oil (PEO): S1 (a, a_1), S2 (b, b_1), S3 (c, c_1), and S4 (d, d_1), acquired at 300× (left column) and 1000× (right column) magnification
Note: Scale bars represent 50 µm and 10 µm, respectively.

The morphological features observed in the present films differ from those reported in some other starch–essential-oil systems. Breadfruit starch films became progressively rougher and more porous as the PEO concentration increased, developing a sponge-like surface at the highest loading [15]. Similarly, potato starch films containing citrus essential oils exhibited rough surfaces, microvoids, and spherical cavity-like features [19]. These studies associated the observed morphological changes with the distribution of the hydrophobic oil phase during film formation and drying. In the present study, however, the available micrographs do not demonstrate an equivalent progressive development of surface cavities across S1–S4. This difference may reflect variations in starch botanical origin, oil composition, formulation, and processing conditions. Nevertheless, because only one specimen and one field of view per magnification were examined for each formulation, the observed differences should be regarded as localized qualitative features rather than representative evidence of systematic morphological changes across the entire film surface.

The identity of the particulate, depression-like, and elongated features cannot be established from the available secondary-electron images alone. In particular, the elongated feature observed in S3 cannot be conclusively assigned to a starch aggregate, residual non-starch constituent, or an oil-associated domain. Likewise, the localized cavity-like features in S2 cannot be definitively identified as pores generated by oil evaporation. The extracted starch contained residual protein (5.56%), crude fiber (2.85%), and ash (1.66%) (Table 1), which represent possible sources of compositional heterogeneity in the starting material. However, their contribution to the individual SEM features remains unverified because no elemental or chemical mapping was available. Accordingly, these features are described morphologically without assigning them to specific chemical constituents or formation mechanisms.

Relatively smooth, homogeneous surfaces have been reported for cassava starch/alginate films containing lemongrass essential oil [21]. PVA/corn starch films containing patchouli oil also showed largely continuous surfaces with few cracks or pinholes [14]. Taken together with the porous surfaces reported in other formulations, these observations suggest that oil concentration alone is insufficient to predict surface morphology across starch–essential oil systems. Polymer composition, oil characteristics, oil dispersion, and film-processing conditions may all influence surface morphology. The SEM observations in the present study provide limited evidence for distinguishing the relative contributions of these factors.

The SEM observations also provide qualitative context for the mechanical measurements discussed in Section 3.3. Although the individual tensile-strength measurements were numerically higher for S3 and S4 than for S1 and S2, the selected SEM fields do not establish a causal relationship between surface morphology and tensile behavior. In particular, surface micrographs cannot demonstrate bulk matrix densification, internal structural continuity, or improved stress transfer through the film. Furthermore, the absence of replicated SEM fields and independent batch-level imaging limits the representativeness of the observed features. Therefore, the SEM results are interpreted as complementary qualitative observations of localized surface morphology rather than direct evidence of the mechanism underlying the measured tensile-strength differences.

3.3 Film thickness and tensile behavior

Film thickness decreased progressively across the four formulations, from 0.53 ± 0.01 mm in S1 to 0.37 ± 0.01 mm in S2, 0.25 ± 0.02 mm in S3, and 0.24 ± 0.01 mm in S4 (Figure 4(a)). This corresponds to an approximately 55% reduction in the measured thickness between S1 and S4. The reported values represent the mean ± standard deviation of three section-level measurements obtained from a single film sheet per formulation, with each section-level value calculated from three individual measurement positions and not batch-to-batch reproducibility. Accordingly, the associated variability reflects spatial differences within the film rather than variation among independently prepared films.

Although the starch and glycerol contents were maintained at 9.75 g and 3.0 mL/100 mL of formulation, respectively, the nominal PEO loading varied across the samples. For each formulation, the entire 100 mL dispersion was cast onto a 20 × 20 cm glass plate, and all films were dried simultaneously under the same oven conditions. Nevertheless, the effective film-covered area, final dry-film mass, and PEO retention after drying were not independently quantified. Consequently, the observed thickness reduction cannot be attributed exclusively to matrix consolidation or changes in polymer-chain packing. Differences in dispersion spreading, component redistribution, and film contraction during drying may also have contributed. This distinction is important because essential-oil incorporation does not produce a uniform thickness response across starch systems.

Kazak and Tuğrul [22], for example, reported increased thickness in corn-, tapioca-, and wheat-starch films, but decreased thickness in potato- and rice-starch films following essential-oil incorporation. These contrasting findings indicate that film thickness depends on the botanical starch source and formulation characteristics. Therefore, the thickness pattern observed here should be interpreted as a descriptive difference among the four PEO-containing formulations rather than definitive evidence of PEO-induced matrix densification.

The tensile-strength measurements showed a numerical increase across the formulation series, from 0.647 MPa in S1 to 0.905 MPa in S2, 1.091 MPa in S3, and 1.215 MPa in S4 (Figure 4(b)). The measured value for S4 was approximately 88% higher than that for S1. However, these values represent individual measurements obtained from one tested specimen per formulation. Consequently, the observed increase is descriptive and does not establish statistically significant differences or demonstrate a reproducible concentration-dependent strengthening effect. Furthermore, because an oil-free starch-glycerol control was not included, the results cannot establish the net effect of PEO incorporation relative to a PEO-free matrix. They instead describe the numerical differences in TS among the four investigated PEO-containing formulations with different nominal PEO loadings.

The mechanical response of starch-based films containing essential oils has been reported to vary considerably with starch source, oil composition, plasticizer content, and processing conditions. TS increased in rice starch films containing oregano essential oil [23]. In starch-chitosan films, TS increased with lemongrass essential oil concentration, although all oil-containing formulations had lower TS than the oil-free control [24]. In corn starch films, increasing the essential oil concentration affected elongation but produced no significant change in TS [25]. Other studies reported lower TS after essential oils were incorporated into starch-based films

[26, 27]. These differences suggest that the effect of essential oils on TS may depend on how the hydrophobic oil phase interacts with the polymer–plasticizer matrix. The specific contribution of PEO to TS in the present formulations remains uncertain.

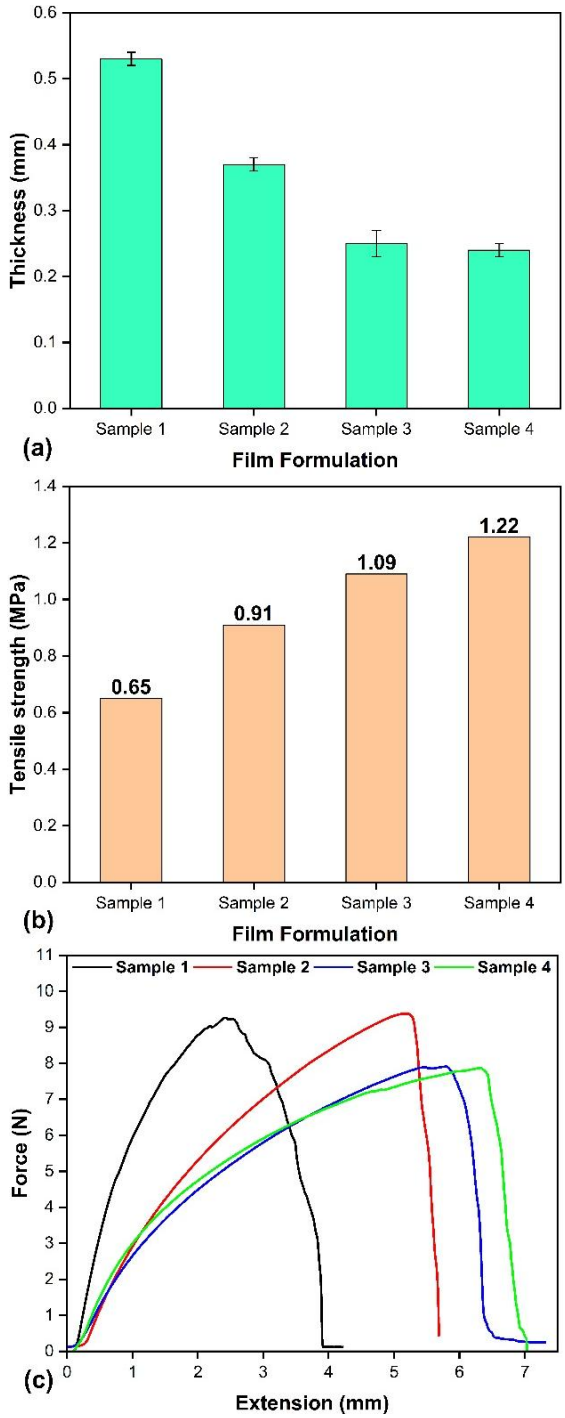

Figure 4. Mechanical and physical properties of durian seed starch films containing different loadings of PEO: (a) film thickness; (b) individual tensile-strength measurements; and (c) force–extension curves for each formulation (S1–S4)
Note: Each section-level value represents the average of three spatial measurements. Error bars in panel (c) indicate within-film spatial variability rather than variation among independently prepared films.

The force–extension curves provide additional context for interpreting the tensile-strength measurements (Figure 4(c)). Among the four investigated formulations, the recorded curves show that S1 and S2 reached higher maximum absolute forces than S3 and S4, despite the latter exhibiting higher calculated tensile-strength values. This apparent discrepancy arises because TS is normalized by the initial cross-sectional area of the specimen, as expressed in Eq. (2). The specimen dimensions reported by the testing laboratory indicate that the initial cross-sectional area decreased across the formulations, primarily because of the reduction in specimen thickness. Consequently, a specimen can exhibit a higher calculated tensile stress while sustaining a lower absolute force at failure. The greater terminal extension observed in the S3 and S4 curves also suggests differences in their recorded deformation behavior; however, these extension values should not be interpreted as elongation at break without the corresponding initial gauge-length information. Overall, the mechanical measurements reveal numerical differences in thickness, TS, and force–extension behavior among the investigated formulations. Nevertheless, these observations should be interpreted descriptively because of the limited number of tested specimens. Further investigations using independently prepared films and multiple tensile specimens are required to establish the reproducibility of these observations and determine whether the observed differences are consistently associated with variations in nominal PEO loading.

3.4 Thermal degradation behavior

Figure 5 shows the TGA and DTG profiles of the durian seed starch films, and Table 3 summarizes the corresponding thermal parameters. All four formulations exhibited broadly similar profiles, with gradual mass loss at lower temperatures followed by a major degradation event at approximately 300–380 °C. The DTG peak temperatures ranged from 319.90 to 326.15 °C, suggesting that the main mass-loss event arose primarily from decomposition of the starch-based matrix. Similar degradation patterns were reported for potato starch films containing citrus essential oils [19] and for ginkgo nut starch films [28], with the main degradation region attributed to the decomposition of starch and plasticizer components. The present TGA and DTG profiles do not resolve the individual contributions of the film constituents.

Differences among the formulations were more apparent in the lower-temperature mass-loss region. The temperature corresponding to 5% mass loss ($T_{5\%}$) ranged from 130.95 to 140.72 °C, with the highest observed value in S3, followed by S2, S1, and S4. A similar pattern was observed for $T_{10\%}$, which increased from 201.04 °C in S1 and 202.01 °C in S2 to 213.72 °C in S3, before decreasing to 192.93 °C in S4. These results indicate non-monotonic differences in the temperatures associated with early mass loss across the four formulations. However, $T_{5\%}$ and $T_{10\%}$ should not be interpreted exclusively as indicators of starch-matrix stability. Pozzebon et al. [29] reported that the initial mass-loss region of corn starch films containing lemongrass essential oil involved overlapping contributions from residual water and volatile essential-oil constituents. A similar consideration applies to the present films because the final moisture content and the amount of PEO retained after film drying were not independently measured. Consequently, the observed differences in $T_{5\%}$ and $T_{10\%}$ may reflect variations in the release of moisture and volatile constituents, together with the onset of thermal decomposition, rather than changes in starch-chain stability alone.

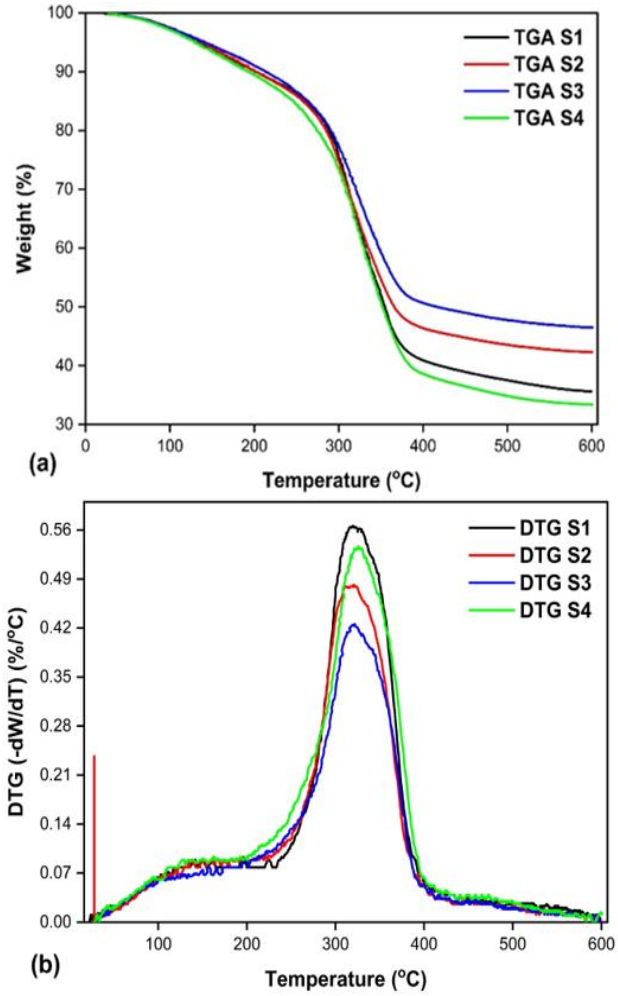

Figure 5. Thermal degradation behavior of durian seed starch films containing different nominal concentrations of patchouli essential oil (PEO): (a) thermogravimetric (TGA) curves and (b) corresponding derivative thermogravimetric (DTG) curve

Note: Each curve represents one individual measurement per formulation (n = 1); DTG profiles were derived from the corresponding TGA data.

The temperature of maximum degradation rate (T_{max}) showed a different numerical pattern, increasing from 319.90 °C in S1 to 320.55 °C in S2, 321.89 °C in S3, and 326.15 °C in S4. Thus, S4 exhibited the highest T_{max}, although the overall difference between S1 and S4 was relatively modest (6.25 °C). The maximum mass-loss rate, however, decreased from 0.57%/°C in S1 to 0.48%/°C in S2 and 0.43%/°C in S3, before increasing to 0.54%/°C in S4. These observations indicate that the temperature of the principal degradation peak and its maximum rate did not follow identical trends. S3 exhibited the lowest maximum mass-loss rate, whereas S4 exhibited the highest T_{max} but a comparatively higher maximum degradation rate than S2 and S3. Similar differences between peak temperature and degradation-rate responses have been reported in starch-based films containing essential oils. Zhou et al. [27], for example, observed changes in the maximum degradation temperature and mass-loss rate in cassava-starch films containing cinnamon essential oil. Such comparisons indicate that thermal degradation characteristics may vary with the starch matrix and formulation. However, because the present measurements were conducted only once per formulation, these differences are descriptive and do not establish statistically significant thermal effects.

The mass remaining at T_{max} and the residual mass at 600 °C provide additional information about the different degradation profiles. At T_{max}, the remaining mass was 65.68% for S1, 66.15% for S2, 69.53% for S3, and 62.14% for S4. S3 therefore exhibited the highest mass remaining at its respective maximum degradation temperature, whereas S4 exhibited the lowest. At 600 °C, the residual mass ranged from 33.39% in S4 to 46.51% in S3, with intermediate values of 35.63% and 42.29% for S1 and S2, respectively. These values represent the residual mass under nitrogen and should not be interpreted directly as either carbonaceous char yield or inorganic ash content. Under an inert atmosphere, the remaining fraction may contain carbonaceous material formed during thermal decomposition together with inorganic constituents that persist at the final temperature. Since no subsequent oxidative treatment or separate ash determination was performed on the films, the relative contributions of these fractions cannot be quantified. Although the extracted starch contained 1.66% ash (Table 1), this value cannot be used directly to determine the inorganic contribution to the final film residue.

The contrasting thermal responses are consistent with previous reports showing that essential oils may influence degradation profiles and residual mass differently depending on the polymer matrix and oil composition. An increase in residual mass was reported for cassava starch films containing cinnamon essential oil [27]. Other starch films containing essential oils exhibited different thermal responses [28, 30]. These findings emphasize that a higher residual mass does not necessarily indicate greater thermal stability or improved packaging performance. In the present study, the relatively high residual mass of S3 and the lower residual mass of S4 describe differences in the outcomes of thermal decomposition under nitrogen, but their practical implications for film performance cannot be established from TGA alone.

Table 3. Thermal degradation parameters of durian seed starch films containing different concentrations of patchouli essential oil (PEO)

Parameter	Unit	S1	S2	S3	S4
$T_{5\%}$	°C	133.38	139.45	140.72	130.95
$T_{10\%}$	°C	201.04	202.01	213.72	192.93
T_{max}	°C	319.90	320.55	321.89	326.15
Maximum mass-loss rate (-dW/dT)	%/°C	0.57	0.48	0.43	0.54
Mass remaining at T_{max}	%	65.68	66.15	69.53	62.14
Residual mass at 600 °C	%	35.63	42.29	46.51	33.39

Note: All values represent individual measurements obtained from one Thermogravimetric analysis (TGA) run per formulation (n = 1), rather than replicate means. Derivative thermogravimetry (DTG) curves were derived from the corresponding TGA data. Mass remaining at T_{max} was obtained from the TGA curve at the temperature corresponding to the maximum DTG rate. Residual mass at 600 °C represents the mass remaining under nitrogen and should not be interpreted as a direct measurement of either carbonaceous char or inorganic ash.

Overall, the single-run thermogravimetric analysis coupled with derivative thermogravimetry (TGA–DTG) profiles revealed distinct but non-monotonic thermal characteristics among the four PEO-containing formulations. S3 exhibited the highest observed $T_{5\%}$ and $T_{10\%}$ values, the lowest maximum mass-loss rate, and the greatest residual mass at 600 °C, whereas S4 exhibited the highest T_{max} but the lowest residual mass. These contrasting observations demonstrate that the thermal response cannot be adequately characterized using a single parameter or interpreted as a progressive improvement in thermal stability with increasing nominal PEO loading. Furthermore, because each formulation was analyzed only once, the reported values represent individual measurements and do not establish experimental reproducibility or statistically significant differences. Accordingly, the results provide a descriptive comparison of the thermal degradation profiles of the investigated formulations rather than definitive evidence of the net thermal effect of PEO incorporation relative to an oil-free starch–glycerol matrix.

3.5 Structure–property relationships

The combined characterization results indicate that the structural, physical, mechanical, and thermal characteristics varied among the four durian seed starch film formulations containing different nominal PEO loadings. The preservation of the main starch-associated FTIR bands, together with the localized surface heterogeneities observed by SEM, suggests that the characteristic features of the starch-based matrix remained detectable across the formulations. However, the available surface micrographs cannot establish bulk matrix densification or a specific stress-transfer mechanism. Similarly, the numerical increase in TS from 0.647 to 1.215 MPa, accompanied by a decrease in film thickness from 0.53 to 0.24 mm, should be interpreted descriptively. Thickness measurements represent spatial variation within individual film sheets, while TS and TGA–DTG measurements were obtained from single specimens or runs per formulation. Consequently, these observations do not establish reproducible mechanical or thermal improvements.

The thermal results further demonstrate that the measured properties did not follow a single concentration-dependent trend. S3 exhibited the highest observed $T_{5\%}$ and $T_{10\%}$ values and the lowest maximum mass-loss rate, whereas S4 showed the highest T_{max}. These differences indicate that early mass loss and the principal degradation event responded differently across the formulations. Nevertheless, the residual mass at 600 °C cannot be interpreted directly as carbonaceous char yield or as an indicator of improved material performance. Taken together, the results suggest formulation-associated variations in the measured properties, but do not establish a single optimum formulation or a definitive molecular mechanism governing these differences.

An important consideration is that the PEO concentrations reported in this study represent nominal initial loadings rather than analytically determined amounts retained in the dried films. PEO was incorporated into the starch dispersion during hot mixing at 90 °C, followed by oven drying at 60 °C for 24 h. Under these processing conditions, partial losses of volatile oil constituents cannot be excluded. However, the retained PEO content was not quantified, and the extent of such losses remains unknown. Accordingly, the observed differences are interpreted in relation to the nominal initial PEO loadings without assuming equivalent oil retention among the dried films. Furthermore, because all formulations contained PEO and no oil-free starch–glycerol control was included, the present results describe differences within the investigated formulation series rather than the net structural or functional effects of PEO addition.

4. CONCLUSIONS

This study investigated the structural, physical, mechanical, and thermal characteristics of durian seed starch films containing four nominal loadings of PEO. The films retained the characteristic starch-associated FTIR bands, while SEM revealed localized surface heterogeneities without a progressive development of extensive cracks or interconnected pores. Across the investigated formulations, film thickness decreased numerically from 0.53 to 0.24 mm, whereas TS increased from 0.647 to 1.215 MPa. The thermal responses were non-monotonic: S3 exhibited the highest observed $T_{5\%}$ and $T_{10\%}$ values and the lowest maximum mass-loss rate, whereas S4 showed the highest T_{max}. These findings indicate that the measured properties varied differently across the nominal PEO loading range, rather than following a uniform improvement in structural, mechanical, or thermal characteristics.

The use of durian seed starch provides a renewable, bio-based feedstock for developing starch-based film materials with potential biodegradability. However, the relatively favorable characteristics observed for S3 are limited to the properties evaluated in this study and should not be interpreted as evidence of superior overall film performance or packaging suitability. Flexibility, moisture resistance, and barrier properties were not directly evaluated, biodegradability was not experimentally assessed, and the amount of PEO retained in the dried films was not quantified. Furthermore, the absence of an oil-free starch–glycerol control and the lack of independent replication for tensile and thermal measurements limit the attribution and generalizability of the observed differences. The durian seeds were also collected during a single collection campaign, pooled into one composite batch, and were not identified by botanical variety; therefore, raw-material variability among independent batches and cultivars was not assessed. Future studies should incorporate matched oil-free controls, independent raw-material collection batches, identified durian varieties, replicated characterization, and direct measurements of PEO retention, flexibility, biodegradability, moisture resistance, and barrier properties. These investigations are necessary to establish the functional potential of durian seed starch–PEO films and assess their possible applications as bio-based packaging materials.

ACKNOWLEDGMENT

The authors gratefully acknowledge the Institute for Research and Community Service (LPPM) of Institut Teknologi Sumatera and the Ministry of Higher Education, Science and Technology of the Republic of Indonesia for financial support through the Penelitian Fundamental Reguler (PFR) research scheme under Contract No. 172/C3/DT.05.00/PL-BARU/2026 and Derivative Contract No. 1416s/DST/IT9.2.1/PT.01.03/2026, both dated 13 April 2026.

REFERENCES

[1] Kacaribu, A.A., Rahmi, R., Julinawati, J., Fathana, H., Reza, M., Iqhramullah, M. (2025). Preparation and characterization of cellulose film from velvet tamarind rind (Dialium indum L.) for food packaging. Applied Science and Engineering Progress, 18(3): 7724. https://doi.org/10.14416/j.asep.2025.03.006

[2] Hidayat, F., Noviyanti, A., Rahmi, R., Indarti, E., Nurman, S., Kacaribu, A.A. (2026). Development of kimpul starch-based composite films reinforced with TEMPO-Oxidized cellulose microfiber for food packaging. Applied Science and Engineering Progress, 19(4): 8101. https://doi.org/10.14416/j.asep.2026.04.001

[3] Dutta, D., Sit, N. (2024). Comprehensive review on developments in starch-based films along with active ingredients for sustainable food packaging. Sustainable Chemistry and Pharmacy, 39: 101534. https://doi.org/10.1016/j.scp.2024.101534

[4] Pei, J.J., Palanisamy, C.P., Srinivasan, G.P., Panagal, M., Kumar, S.S.D., Mironescu, M. (2024). A comprehensive review on starch-based sustainable edible films loaded with bioactive components for food packaging. International Journal of Biological Macromolecules, 274(P1): 133332. https://doi.org/10.1016/j.ijbiomac.2024.133332

[5] Erdiwansyah, Nurman, S., Masyudi, M., et al. (2025). Global trends in agricultural waste-based bioplastic research: A scientometric review. Journal of Human, Earth, and Future, 6(1): 234-246. https://doi.org/10.28991/HEF-2025-06-01-015

[6] Arruda, T.R., Machado, G.D.O., Marques, C.S., et al. (2025). An overview of starch-based materials for sustainable food packaging: Recent advances, limitations, and perspectives. Macromol, 5(2): 19. https://doi.org/10.3390/macromol5020019

[7] Rahmi, Hafiza, U., Julinawati, Febriani, Kacaribu, A.A. (2026). Fabrication of transparent and antimicrobial citric acid crosslinked chitosan-cellulose composite film incorporated with nutmeg oil for food packaging. Next Materials, 11: 101886. https://doi.org/10.1016/j.nxmate.2026.101886

[8] Rahmi, R., Safitri, S., Febriani, F., Lelifajri, L., Kacaribu, A.A. (2026). Fabrication and characterization of cellulose grafted glycidyl methacrylate-based film for food packaging. Baghdad Science Journal, 23(5): 1836-1851. https://doi.org/10.21123/2411-7986.5305

[9] Santhosh, R., Ahmed, J., Thakur, R., Sarkar, P. (2024). Starch-based edible packaging: Rheological, thermal, mechanical, microstructural, and barrier properties-a review. Sustainable Food Technology, 2(2): 307-330. https://doi.org/10.1039/D3FB00211J

[10] Baraheng, S., Karrila, T. (2019). Chemical and functional properties of durian (Durio zibethinus Murr.) seed flour and starch. Food Bioscience, 30: 100412. https://doi.org/10.1016/j.fbio.2019.100412

[11] Gamay, R.A.J., Botecario, P.M.N., Sanchez, P.D.C., Alvarado, M.C. (2024). Durian (*Durio zibenthinus*) waste: A promising resource for food and diverse applications—A comprehensive review. Food Production, Processing and Nutrition, 6(1): 27. https://doi.org/10.1186/s43014-023-00206-4

[12] Ben, Z.Y., Samsudin, H., Yhaya, M.F. (2022). Glycerol: Its properties, polymer synthesis, and applications in starch based films. European Polymer Journal, 175: 111377. https://doi.org/10.1016/j.eurpolymj.2022.111377

[13] van Beek, T.A., Joulain, D. (2018). The essential oil of patchouli, Pogostemon cablin: A review. Flavour and Fragrance Journal, 33(1): 6-51. https://doi.org/10.1002/ffj.3418

[14] Khairan, K., Hasan, M., Idroes, R., Diah, M. (2023). Fabrication and evaluation of polyvinyl alcohol/corn starch/patchouli oil hydrogel films loaded with silver nanoparticles biosynthesized in pogostemon cablin benth leaves' extract. Molecules, 28(5): 2020. https://doi.org/10.3390/molecules28052020

[15] Marta, H., Angelie, K., Yuliana, T., et al. (2026). The effect of patchouli essential oil concentration on physical, mechanical properties and antibacterial activity of breadfruit (*Artocarpus altilis*) starch-based biofilms. Scientific Reports, 16: 33195. https://doi.org/10.1038/s41598-026-67502-0

[16] Rismawati, Elma, Aristyarini, R. (2026). Synthesis and characterization of edible plastic based on waste-derived durian seed starch with patchouli leaf extract as eco-friendly primary packaging. BIO Web of Conferences, 234: 02012. https://doi.org/10.1051/bioconf/202623402012

[17] Irhamni, I., Munandar, A., Saudah, S., et al. (2025). Eco-friendly development of biocomposite films from Durio zibethinus Murr. seeds reinforced with nanocellulose and functional carrageenan additives. Global Journal of Environmental Science and Management, 11(4): 1567-1590. https://doi.org/10.22034/gjesm.2025.04.12

[18] Hidayat, F., Indarti, E., Rahmi, Arahman, N. (2025). Synthesis of a biocomposite based on Kluwih (Artocarpus camansi) seed starch incorporated with carrageenan as a functional additive and cellulose nanofiber filler. Case Studies in Chemical and Environmental Engineering, 11: 101120. https://doi.org/10.1016/j.cscee.2025.101120

[19] Lemos, J.M., Lopes, J.E.M., Rangel, J.H.G., et al. (2026). Active starch films incorporated with citrus essential oils: Properties, bioactivity, and biodegradability. Polymers, 18(14): 1794. https://doi.org/10.3390/polym18141794

[20] Guo, Y.B., Zhang, B.J., Zhao, S.M., Qiao, D.L., Xie, F.W. (2021). Plasticized starch/agar composite films: Processing, morphology, structure, mechanical properties and surface hydrophilicity. Coatings, 11(3): 311. https://doi.org/10.3390/coatings11030311

[21] Torres Vargas, O.L., Galeano Loaiza, Y.V., Rodríguez Agredo, I.A. (2024). Development and characterisation of starch/alginate active films incorporated with lemongrass essential oil (Cymbopogon citratus). Materials Advances, 5(23): 9417-9427. https://doi.org/10.1039/D4MA00608A

[22] Kazak, M.B., Tugrul, N. (2024). Comparison of the film properties of lemon and sour cherry seed essential oil-added glycerol and/or sorbitol-plasticized corn, potato, rice, tapioca, and wheat starch-based edible films. International Journal of Polymer Science, 2024: 9112555. https://doi.org/10.1155/2024/9112555

[23] Martins, P.C., Bagatini, D.C., Martins, V.G. (2021). Oregano essential oil addition in rice starch films and its effects on the chilled fish storage. Journal of Food Science and Technology, 58(4): 1562-1573.

https://doi.org/10.1007/s13197-020-04668-z
[24] Manshor, N.M., Samsudin, S., Yahya, A., Ahmad Zamanhuri, N., Raslan, R. (2026). Physicochemical properties of starch-chitosan film with lemongrass essential oil. ASEAN Journal of Chemical Engineering, 26(1): 92-104. https://doi.org/10.22146/ajche.21037
[25] Ghasemlou, M., Aliheidari, N., Fahmi, R., et al. (2013). Physical, mechanical and barrier properties of corn starch films incorporated with plant essential oils. Carbohydrate Polymers, 98(1): 1117-1126. https://doi.org/10.1016/j.carbpol.2013.07.026
[26] Wang, B., Sui, J., Yu, B., et al. (2021). Physicochemical properties and antibacterial activity of corn starch-based films incorporated with Zanthoxylum bungeanum essential oil. Carbohydrate Polymers, 254: 117314. https://doi.org/10.1016/j.carbpol.2020.117314
[27] Zhou, Y., Wu, X.H., Chen, J.H., He, J.H. (2021). Effects of cinnamon essential oil on the physical, mechanical, structural and thermal properties of cassava starch-based edible films. International Journal of Biological Macromolecules, 184: 574-583. https://doi.org/10.1016/j.ijbiomac.2021.06.067
[28] Kim, B.K., Lee, H.S., Yang, H.S., Song, K.B. (2021). Development of ginkgo (Ginkgo biloba) nut starch films containing cinnamon (Cinnamomum zeylanicum) leaf essential oil. Molecules, 26(20): 6114. https://doi.org/10.3390/molecules26206114
[29] Pozzebon, G., Gauger, L.R., Francisquetti, E.L., Yudice, E.D.C., Borsoi, C., Romanzini, D. (2026). High-shear processing of surfactant-free corn starch films: Impact of lemongrass essential oil on structural and antibacterial performance. Polymer Bulletin, 83(6): 288. https://doi.org/10.1007/s00289-026-06351-3
[30] Criollo-Feijoo, J., Salas-Gomez, V., Cornejo, F., Auras, R., Salazar, R. (2024). Cassava bagasse starch and oregano essential oil as a potential active food packaging material: A physicochemical, thermal, mechanical, antioxidant, and antimicrobial study. Heliyon, 10(16): e36150. https://doi.org/10.1016/j.heliyon.2024.e36150